Journal of Applied Physics

RESEARCH ARTICLE | MAY 08 2025

# Investigation of the structural, electronic, magnetic, and mechanical characteristics of double half-Heusler alloys $V_2Ni_2Z'Z''$ ($Z'$ = Al, Ga and $Z''$ = Sb, Sn) using *ab initio* computational methods

Nurpeiis A. Merali ; Nurgul S. Soltanbek ; Nursultan E. Sagatov ; Aisulu U. Abuova ; Vladimir V. Khovaylo ; Fatima U. Abuova ; Talgat M. Inerbaev



*J. Appl. Phys.* 137, 185101 (2025)
https://doi.org/10.1063/5.0252730







AIP Publishing

Journal of Applied Physics ARTICLE pubs.aip.org/aip/jap

# Investigation of the structural, electronic, magnetic, and mechanical characteristics of double half-Heusler alloys $V_2Ni_2Z'Z''$ ($Z'$ = Al, Ga and $Z''$ = Sb, Sn) using *ab initio* computational methods

Cite as: J. Appl. Phys. **137**, 185101 (2025); doi: 10.1063/5.0252730
Submitted: 11 December 2024 · Accepted: 22 April 2025 ·
Published Online: 8 May 2025



Nurpeiis A. Merali,[1] Nurgul S. Soltanbek,[1,a)] Nursultan E. Sagatov,[2] Aisulu U. Abuova,[1] Vladimir V. Khovaylo,[3] Fatima U. Abuova,[1,a)] and Talgat M. Inerbaev[1,4]

## AFFILIATIONS

[1]L. N. Gumilyov Eurasian National University, Astana 010000, Republic of Kazakhstan
[2]Sobolev Institute of Geology and Mineralogy, Siberian Branch of the Russian Academy of Sciences, Novosibirsk 630090, Russian Federation
[3]National University of Science and Technology "MISIS," Moscow 119049, Russian Federation
[4]Vernadsky Institute of Geochemistry and Analytical Chemistry RAS, Moscow 119991, Russian Federation

[a)]**Authors to whom correspondence should be addressed:** sns.nurgul@mail.ru and abuova_fu@enu.kz



## ABSTRACT

The electronic, magnetic, elastic, and vibrational properties of new double half-Heusler (DHH) alloys $V_2Ni_2Z'Z''$ are investigated within the density functional theory (DFT) calculations. All investigated alloys demonstrated mechanical, dynamic, and thermodynamic stability and complied with the Slater–Pauling rule. The analysis of their magnetic states indicates that all DHH alloys under investigation exhibit a ferromagnetic ground state. Electronic property analysis reveals that each alloy behaves as a half-metal, with an energy gap in the spin-up channel ranging from 0.103 to 0.653 eV. Based on the $B/G$ ratio, the brittleness–ductility assessment yielded values around 2.5, indicating that alloys are ductile. The combination of magnetic properties, half-metallicity, and mechanical resilience makes these $V_2Ni_2Z'Z''$ alloys promising candidates for high-performance spintronics devices and other advanced technological applications.



## I. INTRODUCTION

Recent attention has focused on double half-Heusler (DHH) alloys such as ($X'X''Y_2Z_2$, $X_2Y'Y''Z_2$, and $X_2Y_2Z'Z''$) because of their special structural symmetry with complex electronic properties, different from conventional Heusler compounds.[1,2] The transition metals X and Y, along with the main group elements Z in Heusler alloys, make it one of the potential alloys for new electronic discoveries and various multifunctional applications. Unlike the $X_2YZ$ full- and XYZ half-Heusler alloys that have been studied in some detail, the DHH alloys exhibit a unit cell, which is doubled and, because of the presence of aliovalent elements Y′ and Y″, structurally even more complicated.[3–7] With this particular arrangement, the DHH alloys exhibit huge potential candidates for advanced electronic properties and applications in state-of-the-art technologies, like spintronics or thermoelectrics, and are, thus, one of the central topics in modern materials research.

Anand *et al.*[2] propose that the thermal conductivity ($\kappa$) in double half-Heusler compounds is primarily governed by reduced group velocity phonons and constrained by disorder scattering effects, which should reduce $\kappa$ compared to contemporary ternary half-Heusler thermoelectric materials, whose efficiency is hindered

by their inherently high $\kappa$. Through the synthesis of $Ti_2FeNiSb_2$, they have demonstrated and validated that this DHH alloy exhibits markedly lower thermal conductivity than its ternary half-Heusler analog TiCoSb, thus presenting a superior foundation for the enhancement of thermoelectric efficiency.[2] Rached *et al.*[8] compared the structural, thermoelectric, and elastic properties of identical half (TiXSb, X = Ru, Pt) and double half-Heusler alloys ($Ti_2RuPtSb_2$). The authors have determined through computational analysis that the $Ti_2RuPtSb_2$ compound exhibits pronounced peaks in the absorption coefficient within the ultraviolet (UV) spectral range, suggesting its potential utility as UV filters and UV photodetectors. The investigated materials have also demonstrated promising thermoelectric properties, indicating their suitability as potential candidates for thermoelectric device applications.[8–13] In most instances, double half-Heusler alloys exhibit semiconductor behavior,[14] exemplified by the investigations conducted by Bouhadjer *et al.*[15] In their study, $Ti_2FeNiSb_2$ and $Ti_2Ni_2InSb$ alloys were observed, displaying bandgap energies of 0.64 and 0.43 eV, respectively. Ding *et al.*[16] developed a half-metallic alloy $Mn_2FeCoSi_2$ and studied its electronic and magnetic properties. The effect of different types of disorder on the half-metallic properties of $Mn_2FeCoSi_2$ was also investigated. Douinat *et al.*[17] conducted a study on the alloys $Zr_2AlBiNi_2$ and $Zr_2GaBiNi_2$, demonstrating their stability through *ab initio* calculations. These alloys exhibit typical semiconductor behavior with direct bandgaps of 0.540 and 0.496 eV. According to the obtained data, these alloys could be considered potential candidates for applications in electronics, optics, and communication. Cui *et al.*[18] studied two double half-Heusler alloys, $Mn_2CoCrP_2$ and $Mn_2CoCrAs_2$. They were found to be half-metallic ferrimagnets with a relatively large spin-down bandgap. The work also showed that their magnetic moments and half-metallic properties increase their resistance to the effect of tetragonal distortion. In addition, the authors modeled two types of magnetic tunnel junctions using a double half-Heusler alloy as electrodes and GaAs as a barrier. By calculating the Fermi-level transmittances, the authors show that both devices exhibit high conductivity when the magnetic moments of the two magnetic electrodes are connected in parallel. In contrast, when the magnetic moments of the two electrodes are arranged antiparallel, the electron transport capacity of the lower spin emitters is significantly suppressed. Thus, in addition to their use as thermoelectric materials, double half-Heusler alloys are promising candidates for high-performance spintronic devices.

Despite the advantages and large number of double half-Heusler alloys that have been extensively studied over the past decade,[19–23] many new compound combinations have not been investigated experimentally or theoretically. This study represents the first extensive investigation of the structural, electronic, magnetic, and mechanical and phonon properties, including chemical bonding characteristics, of the previously unexplored double half-Heusler compounds $V_2Ni_2Z'Z''$ (where $Z' =$ Al, Ga and $Z'' =$ Sb, Sn). The present results will enhance the understanding of their physicochemical properties and help to assess the possible use of the alloys in advanced technological applications, especially in the area of spintronics. This study distinguishes itself from previous studies by introducing and characterizing novel compositions, thereby expanding the known landscape of double half-Heusler materials.

## II. COMPUTATIONAL METHODS

The calculations were performed using the Vienna *Ab initio* Simulation Package (VASP) within the density functional theory (DFT) methodology[24,25] and have been effectively employed in the calculation of other functional materials.[26–30] All calculations were performed using the generalized gradient approximation (GGA) within the Perdew–Burke–Ernzerhof functional (PBE) to account for the exchange-correlation interaction.[31] However, for electronic properties, since standard DFT functionals are known to underestimate the bandgap, we employed the meta-GGA functional, namely, SCAN, to achieve a more accurate description.[32] A baseline plane wave cutoff of 700 eV was applied in all instances. The integration of the Brillouin zone was achieved through a grid of $12 \times 12 \times 6$ k points. These parameter choices demonstrated satisfactory convergence in total energy. Convergence tolerance for the calculations was set at a total energy difference within the range of $10^{-7}$ eV/atom. The charge distribution on the ions was investigated employing topological analysis, utilizing the Bader method. The phonon calculations were performed using PhonoPy program.[33] Real-space force constants were calculated using supercell and finite displacement approaches, with $2 \times 2 \times 1$ supercells for all considered compounds. The elastic stiffness tensor ($C_{ij}$) of the compounds considered was calculated using the stress ($\sigma$)–strain ($\epsilon$) relation $\sigma_i = C_{ij}\epsilon_j$, and from the obtained data, all desired mechanical properties were estimated. To describe elastic properties, we use Voigt[34] and Reuss[35] equations. For a tetragonal crystal, the bulk and shear modulus by the Voigt ($B_V$,$G_V$) and the Reuss averaging ($B_R$, $G_R$) can be derived from the elastic constants as follows:

$$B_V = \frac{2(C_{11} + C_{12}) + C_{33} + 4C_{13}}{9},$$

$$G_V = \frac{M + 3C_{11} - 3C_{12} + 12C_{44} + 6C_{66}}{30},$$

$$B_R = \frac{(C_{11} + C_{12})C_{33} - 2C_{13}^2}{M},$$

$$G_R = 15 \Bigg/ \left\{ \frac{18B_V}{C^2} + \left[ \frac{6}{(C_{11} - C_{12}) + \left(\frac{6}{C_{44}}\right) + \left(\frac{3}{C_{66}}\right)} \right] \right\},$$

where $C^2 = (C_{11} + C_{12})C_{33} - C_{13}^2$; $M = C_{11} + C_{12} + 2C_{33} - 3C_{13}$.

Following Hill's guidelines,[36,37] the volume and shear moduli were estimated by averaging the upper and lower bounds, applying the equations provided below:

$$B = \frac{B_V + B_R}{2}; \quad G = \frac{G_V + G_R}{2}.$$

Young's modulus,[38] Poisson's ratio,[39] and melting temperature[40,41] were determined using the equations provided below:

$$E = \frac{9BG}{3B + G}; \; \nu = \frac{3B - 2G}{(2 * (3B + G)}; \; T_m = 354 + \frac{2}{3} \cdot (2C_{11} + C_{33}).$$

To calculate the Vickers hardness of the alloys under investigation, we used the empirical models proposed by Chen[42] and Tian,[43]

$$H_V^{Chen} = 2 \cdot (k^2 \cdot G)^{0.585} - 3,$$

$$H_V^{Tian} = 0.92 \cdot k^{1.137} \cdot G^{0.708},$$

where $k = G/B$. In our study, $H_V$ was calculated using the average value obtained from $H_V^{\mathrm{Chen}}$ and $H_V^{\mathrm{Tian}}$,

$$H_V = \frac{H_V^{Chen} + H_V^{Tian}}{2}.$$

In this study, we used Belomestnykh's formalism to calculate the Grüneisen parameter ($\gamma^{ac}$) using the longitudinal ($v_l$) and transverse ($v_s$) acoustic wave velocities,

$$\gamma^{ac} = \frac{3}{2}\frac{\left(3v_l^2 - 4v_t^2\right)}{\left(v_l^2 + 2v_t^2\right)}.$$

## III. RESULTS AND DISCUSSION

### A. Structural and magnetic properties

The DHH compounds $V_2Ni_2Z'Z''$ (where Z′ = Al, Ga and Z″ = Sb, Sn) are typically considered within a body-centered tetragonal structure belonging to the $I\bar{4}2d$ space group (No.122). As it is shown in Fig. 1, the X, Y, Z′, and Z″ atoms locate at (0, 0.5, 0.495), (0.75, 0.25, 0.625), (0, 0.5, 0.25), and (0, 0, 0.5) sites, respectively. In this arrangement, the X (V) and Y (Ni) atoms are located at the 8*c* and 8*d* sites, while the Z′ (Al, Ga) and Z″ (Sn, Sb) atoms occupy the 4*a* and 4*b* Wyckoff positions.

The enthalpy of formation for the studied chemical compounds, excluding zero-point energy corrections, was determined. The enthalpy of formation was computed using the following formula:

$$\Delta H(X_2Y_2ZZ') = H(X_2Y_2ZZ') - [2H(X) + 2H(Y) + H(Z) + H(Z')].$$

Table I presents the optimized parameters and computed formation enthalpies for the studied compounds. All enthalpy values are negative, suggesting thermodynamic stability and a favorable experimental synthesis route for each compound. Notably, experimental formation enthalpies are not currently available for $V_2Ni_2Z'Z''$ (where Z′ = Al, Ga and Z″ = Sb, Sn) compounds.

Table II also demonstrates that the Slater–Pauling rule, formulated for double half-Heusler alloys as $M_t = Z_t - 36$, accurately predicts the total magnetic moment for the alloys studied. An examination of the magnetic properties of materials reveals that V atoms exhibit the highest atomic spin magnetic moment (AMM), ranging from 0.42 to 0.99 $\mu_B$, indicating their dominant contribution to the total spin magnetic moment. Both V and Ni atoms possess positive AMM values, resulting in a parallel arrangement of their magnetic moments. In contrast, the Z′ and Z″ atoms contribute minimally, with small negative magnetic moments between −0.03 and −0.07 $\mu_B$. All DHH alloys investigated exhibit a ferromagnetic ground state, characterized by the alignment of atomic magnetic moments in a parallel orientation, driven by exchange interaction mechanisms.

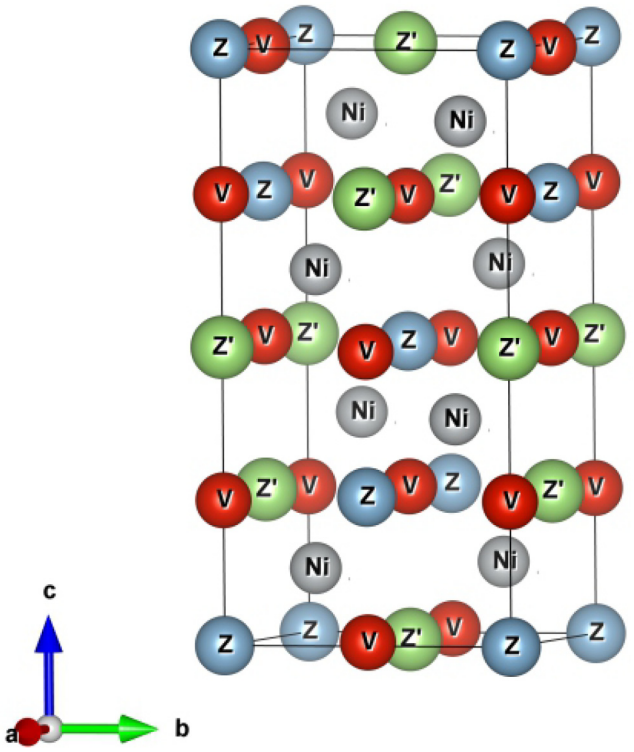


FIG. 1. Crystal structure of double half $V_2Ni_2Z'Z''$ alloys (Z′ = Al, Ga and Z″ = Sb, Sn).

### B. Vibrational properties

Figure 2 shows the phonon dispersion curves and the corresponding phonon DOS, which give an idea of the vibration behavior and dynamic stability of the material. The dynamic stability of $V_2Ni_2Z'Z''$ alloys was assessed by analyzing their vibrational properties, in particular, through phonon dispersion curves and phonon density of states (DOS).

TABLE I. Structural information for $V_2Ni_2Z'Z''$ compounds.

| Compounds | $a = b$, Å | $c$, Å | $\Delta H$, eV/f.u. |
|---|---|---|---|
| $V_2Ni_2AlSb$ | 5.740 | 11.476 | −1.44 |
| $V_2Ni_2AlSn$ | 5.729 | 11.435 | −1.35 |
| $V_2Ni_2GaSb$ | 5.738 | 11.447 | −1.40 |
| $V_2Ni_2GaSn$ | 5.726 | 11.404 | −1.31 |

**TABLE II.** Evaluated parameters of the magnetic moment of each atom ($\mu$), predicted magnetic moments by Slater–Pauling rule ($M_t$), total magnetic moments ($\mu$), magnetic type $V_2Ni_2Z'Z''$ (Z′ = Al, Ga and Z″ = Sb, Sn) compounds.

| Compounds | $\mu$, atom (V) | $\mu$, atom (Ni) | $\mu$, atom (Z′) | $\mu$, atom (Z″) | $M_t$ | $\mu$, total | Magnetic state |
|---|---|---|---|---|---|---|---|
| $V_2Ni_2AlSb$ | 0.975 | 0.077 | −0.029 (Al) | −0.038 (Sb) | 2 | 1.964 | FM |
| $V_2Ni_2AlSn$ | 0.430 | 0.011 | −0.014 (Al) | −0.029 (Sn) | 1 | 0.843 | FM |
| $V_2Ni_2GaSb$ | 0.992 | 0.022 | −0.039 (Ga) | −0.067 (Sb) | 2 | 2.083 | FM |
| $V_2Ni_2GaSn$ | 0.420 | 0.010 | −0.028 (Ga) | −0.032 (Sn) | 1 | 0.846 | FM |

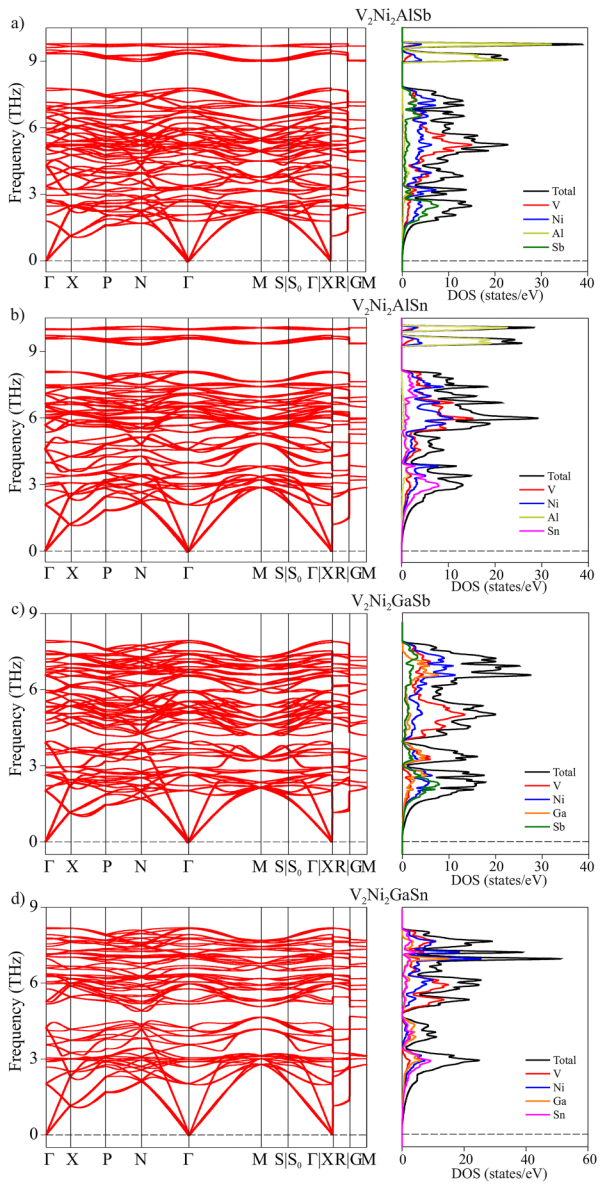


**FIG. 2.** Calculated phonon dispersion curves and phonon density of states for $V_2Ni_2ZZ'$ compounds.

Each compound contains 12 atoms per primitive cell, leading to 36 vibrational modes in the phonon band structure, represented as $M = 2A_1 + 3A_2 + 4B_1 + 5B_2 + 11E$. The first three acoustic modes ($\Gamma_{acoustic} = B_2 + E$) correspond to the collective movement of the center of mass, whereas the optical modes ($\Gamma_{optic} = 2A1 + 3A_2 + 4B_1 + 4B_2 + 10E$) describe relative atomic motion. Group theory analysis reveals 30 Raman active modes ($\Gamma_{Raman} = 2A_1 + 4B_1 + 4B_2 + 10E$), 24 infrared (IR) active modes ($\Gamma_{IR} = 4B_2 + 10E$), and 3 silent modes ($\Gamma_{Silent} = 3A_2$) in $V_2Ni_2Z'Z''$ alloys. The vibrational modes at the Γ-point are listed in Table III. In the analysis of the phonon density of states (DOS), a phonon bandgap is observed in $V_2Ni_2AlSb$ and $V_2Ni_2AlSn$ alloys from 8 to 9.5 THz, while no bandgap appears in $V_2Ni_2SnSn$ from

**TABLE III.** Calculated optical modes ($\omega$) of $V_2Ni_2Z'Z''$ (Z′ = Al, Ga and Z″ = Sb and Sn), their activity and corresponding Mulliken symbols. Here, 1 is $V_2Ni_2AlSb$, 2 is $V_2Ni_2AlSn$, 3 is $V_2Ni_2GaSb$, and 4 is $V_2Ni_2GaSn$.

| Mul. sym. | Activity | $\omega$ (THz) 1 | 2 | 3 | 4 |
|---|---|---|---|---|---|
| $E$ | Raman, IR | 2.755 | 2.775 | 2.629 | 2.681 |
| $E$ | Raman, IR | 3.231 | 3.311 | 2.917 | 2.975 |
| $B_1$ | Raman | 2.469 | 2.915 | 2.211 | 2.910 |
| $B_2$ | Raman, IR | 2.952 | 4.001 | 2.144 | 3.546 |
| $A_2$ | Silent | 4.523 | 6.002 | 4.358 | 6.056 |
| $A_1$ | Raman | 5.170 | 6.317 | 5.068 | 6.282 |
| $A_2$ | Silent | 5.242 | 6.277 | 5.343 | 6.255 |
| $E$ | Raman, IR | 4.264 | 4.549 | 3.669 | 3.904 |
| $B_1$ | Raman | 3.876 | 4.907 | 3.506 | 4.129 |
| $E$ | Raman,IR | 4.806 | 5.345 | 4.671 | 5.174 |
| $B_2$ | Raman, IR | 5.975 | 6.536 | 5.891 | 6.339 |
| $E$ | Raman, IR | 5.314 | 6.037 | 5.308 | 5.974 |
| $E$ | Raman, IR | 6.708 | 7.090 | 5.973 | 6.291 |
| $B_2$ | Raman, IR | 7.149 | 7.489 | 6.804 | 7.162 |
| $B_1$ | Raman | 6.481 | 7.024 | 6.567 | 6.971 |
| $E$ | Raman, IR | 6.980 | 7.349 | 6.697 | 7.049 |
| $A_1$ | Raman | 6.216 | 6.661 | 6.526 | 6.693 |
| $A_2$ | Silent | 6.445 | 7.107 | 6.682 | 7.098 |
| $E$ | Raman, IR | 7.785 | 8.101 | 7.101 | 7.352 |
| $E$ | Raman, IR | 9.334 | 9.583 | 7.429 | 7.919 |
| $B_2$ | Raman, IR | 9.612 | 9.968 | 7.210 | 7.550 |
| $E$ | Raman, IR | 9.505 | 9.718 | 7.934 | 8.188 |
| $B_1$ | Raman | 9.779 | 10.012 | 7.083 | 7.452 |

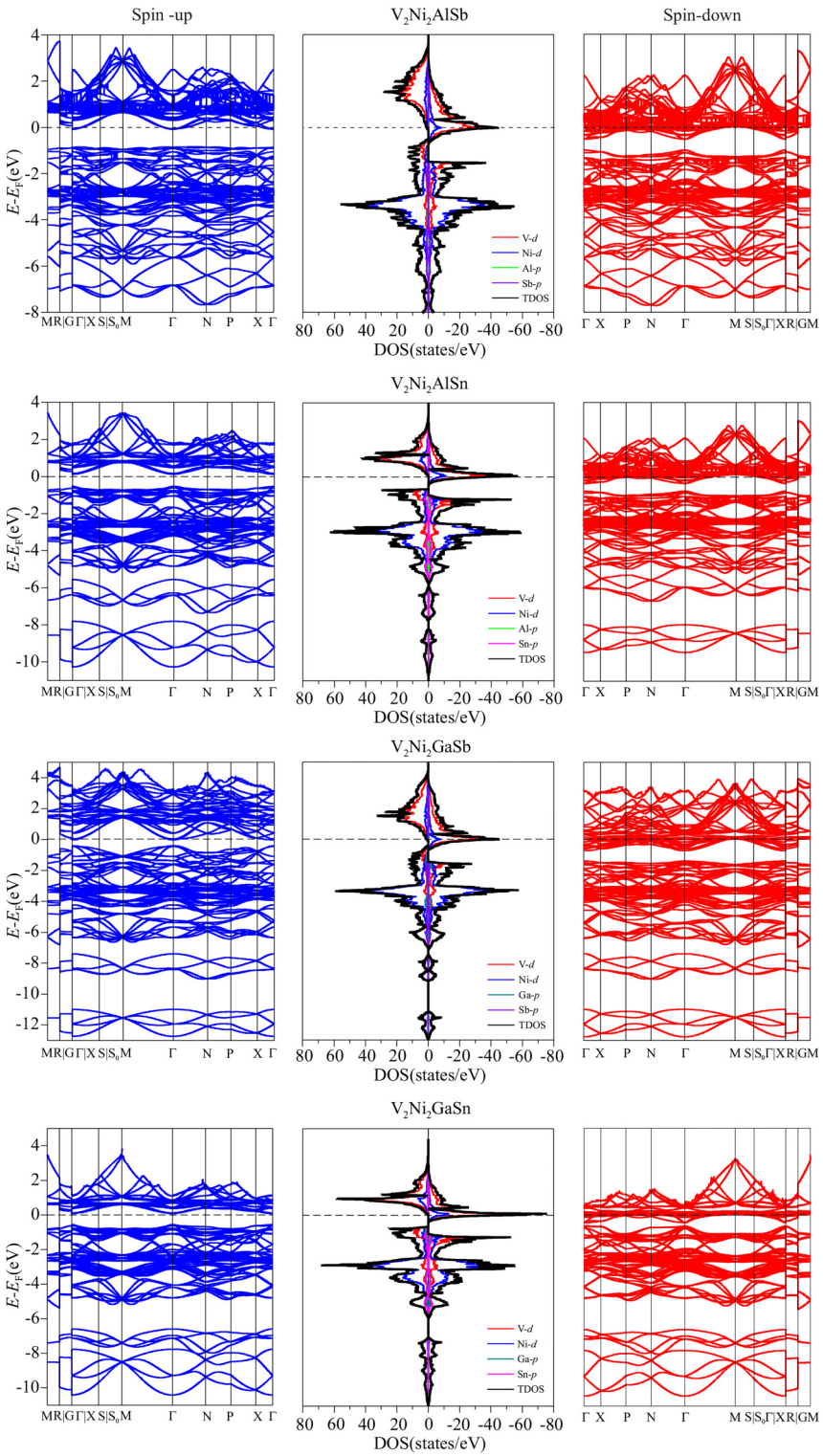


**FIG. 3.** The density of states and electronic band structure of the $V_2Ni_2Z'Z''$ double half-Heusler alloys.

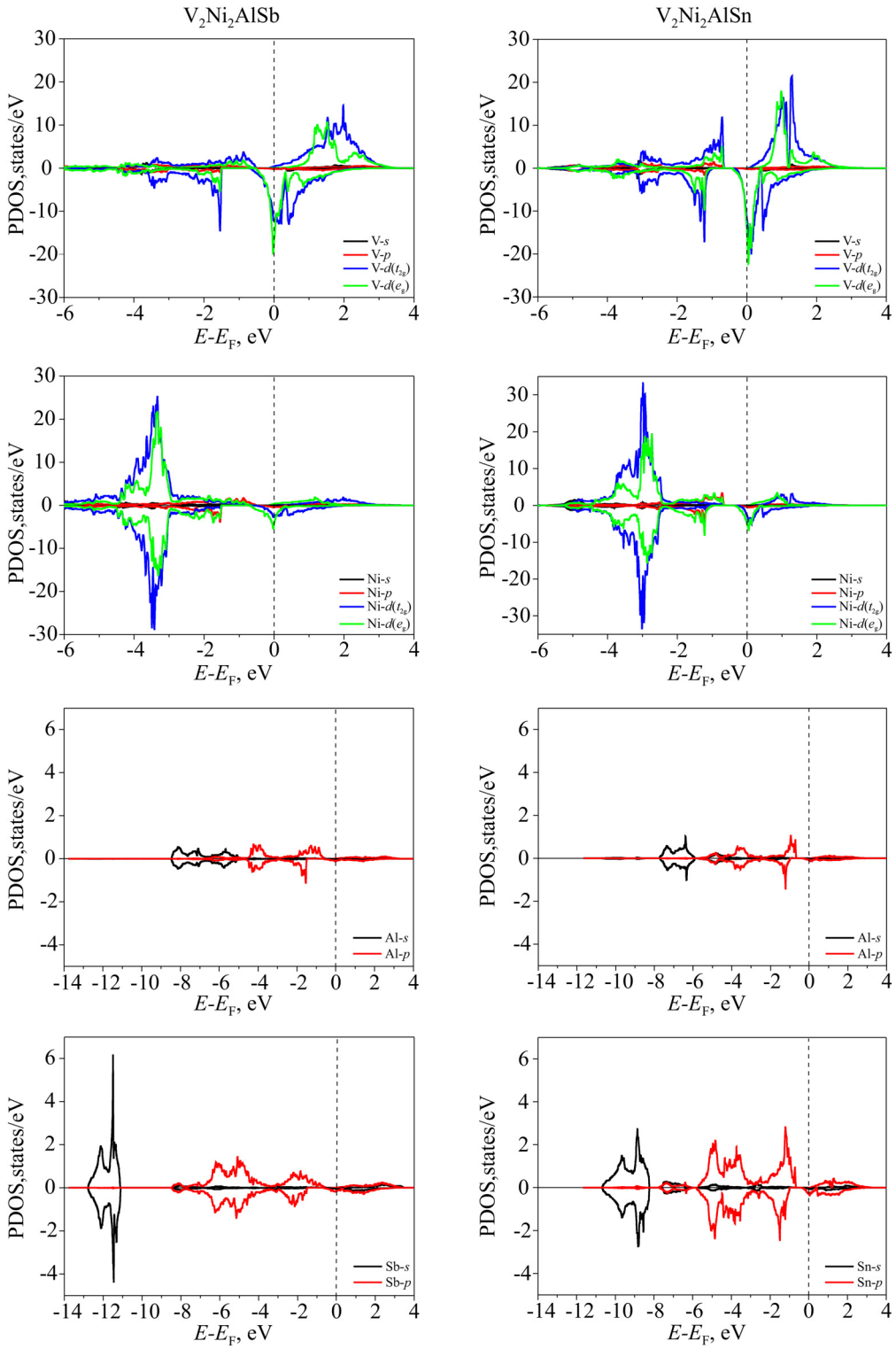


**FIG. 4.** The partial density of states for $V_2Ni_2AlSb$ and $V_2Ni_2AlSn$ structures. Zero on the energy axis corresponds to the Fermi level.

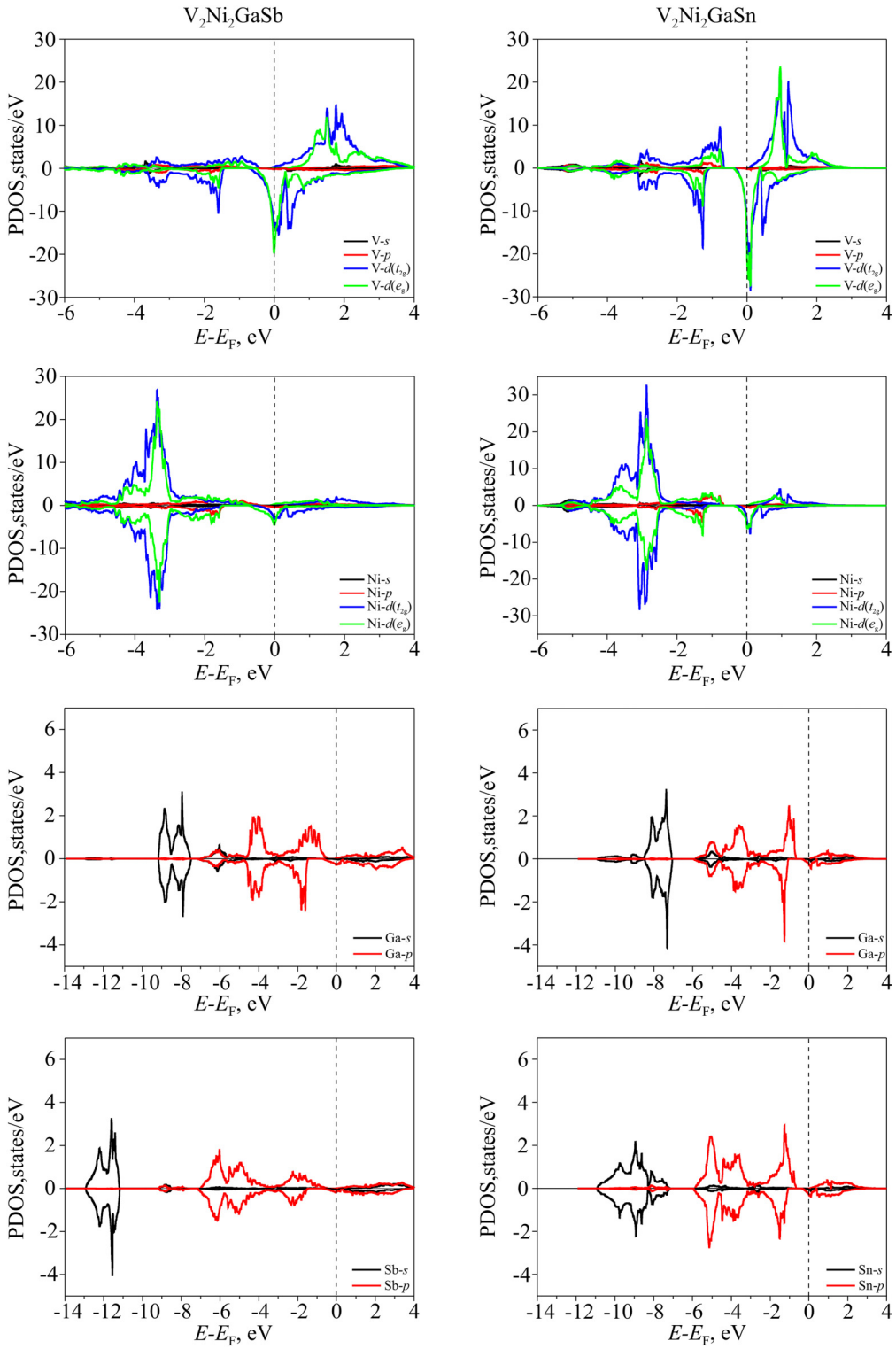


**FIG. 5.** The partial density of states for $V_2Ni_2GaSb$ and $V_2Ni_2GaSn$ structures. Zero on the energy axis corresponds to the Fermi level.

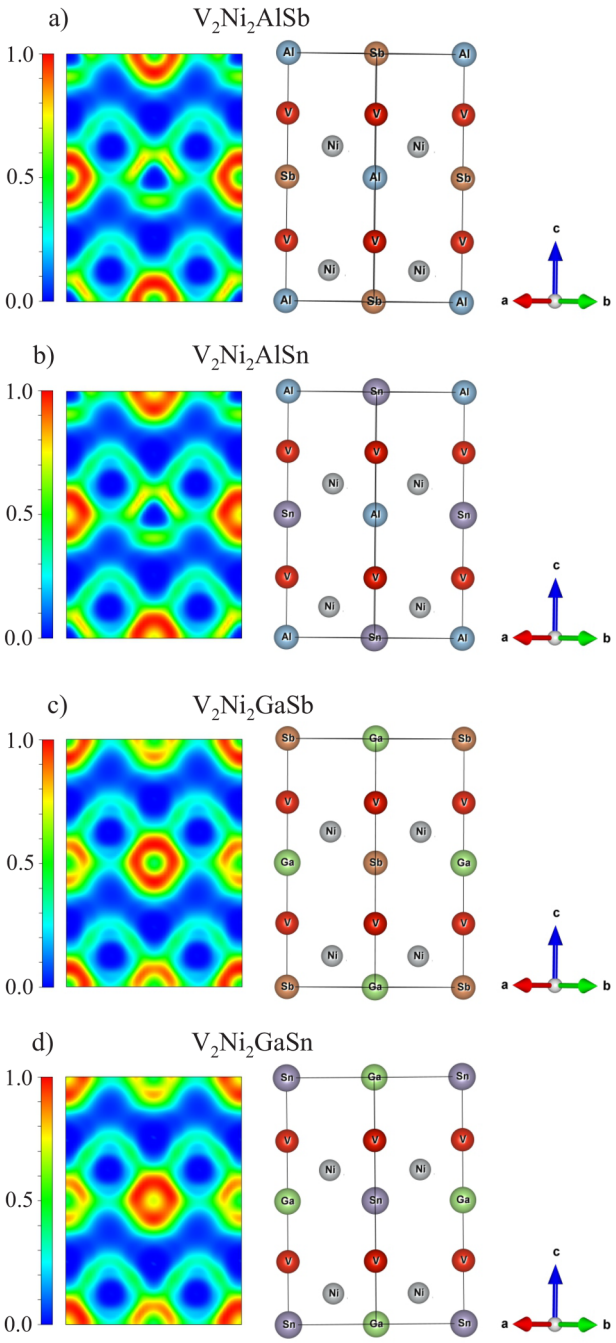


**FIG. 6.** Calculation of ELF of the $V_2Ni_2Z'Z''$ double half-Heusler alloys in the (110) plane.

4.5 to 5 THz, nor in $V_2Ni_2GaSb$. V atoms make a dominant contribution to the total phonon DOS in the 5.5–7 THz range, whereas Al atoms predominantly contribute from 9 to 9.5 THz, with other atoms contributing uniformly across these ranges.

**TABLE IV.** Calculated elastic constants $C_{ij}$ for $V_2Ni_2Z'Z''$ compounds in GPa.

| Compounds | $C_{11}$ | $C_{12}$ | $C_{13}$ | $C_{33}$ | $C_{44}$ | $C_{66}$ |
|---|---|---|---|---|---|---|
| $V_2Ni_2AlSb$ | 209.0 | 97.7 | 96.8 | 204.1 | 58.5 | 53.4 |
| $V_2Ni_2AlSn$ | 218.6 | 96.4 | 95.2 | 216.6 | 59.1 | 58.4 |
| $V_2Ni_2GaSb$ | 202.3 | 103.0 | 102.8 | 200.2 | 57.4 | 52.5 |
| $V_2Ni_2GaSn$ | 213.1 | 101.5 | 101.1 | 212.9 | 59.1 | 59.5 |

The absence of imaginary phonon modes throughout the Brillouin zone in the phonon dispersion calculations confirms that atoms in these alloys return to their equilibrium positions upon disturbance, indicating that the $V_2Ni_2Z'Z''$ alloys are dynamically stable.

## C. Electronic properties

The density of states (DOS) serves as a crucial parameter in characterizing energy levels. The computed band structure and DOS are presented in Fig. 3. Analysis of the four plots reveals that the Ni atom's *d*-states predominantly contribute to the total density of states in the lower region of the valence band, specifically between approximately −4 and −3 eV. In contrast, at the upper edge of the conduction band, around 1–2.5 eV, the unoccupied *d*-states of the V atom play a significant role. According to the results, the highest energy level in the valence band maximum (VBM) and the lowest energy level in the conduction band minimum (CBM) are both located at point Γ. The band profiles are similar for all four compounds. The density of states (DOS) analysis and band structure examination revealed the presence of a bandgap near the Fermi level. Among the alloys studied, the $V_2Ni_2AlSb$ alloy exhibited the largest bandgap, measured at 0.613 eV. In contrast, the $V_2Ni_2GaSb$ alloy showed the smallest bandgap, recorded at 0.103 eV. The bandgap values in the remaining two alloys were observed to fluctuate around 0.235 eV. Additionally, an energy gap is observed in the $\alpha$-states of $V_2Ni_2Z'Z''$ Heusler alloys near the Fermi level, indicating half-metallic characteristics of the alloy.

The projected density of states (PDOS) for the examined $V_2Ni_2Z'Z''$ structures is illustrated in Figs. 4 and 5. For each Heusler alloy composition, the *p*-orbital contributions from the Ga and Sn atoms are primarily localized at lower energy levels, around −6 eV. In contrast, the *p*-orbital contributions from Al and Sb atoms are notably minimal across these energy ranges. This distribution suggests a distinctive separation in the electronic structure, with Ga and Sn atoms contributing significantly at lower energies, while Al and Sb atoms play a less prominent role. This observation aligns with the electronic configuration and bonding characteristics observed across the Heusler alloy systems under investigation. In the alloy structures $V_2Ni_2AlSb$ and $V_2Ni_2AlSn$, the projected density of *d*-states for Ni atoms reveals an energy gap near the Fermi level, as illustrated in Fig. 4. This feature indicates the formation of a half-metallic electronic structure within both alloys. This half-metallicity arises from the contributions of $e_g$ ($\alpha$) and $t_{2g}$ ($\beta$) states in the V atoms, which play a central role in defining the electronic behavior near the Fermi level. These findings highlight the

**TABLE V.** Evaluated parameters of the bulk (in GPa), shear (in GPa), Young's (in GPa) moduli, Poisson's ratio, *B*/*G* ratio, Vickers hardness (in GPa), fracture toughness (in MPa $m^{1/2}$), shear anisotropic factors $A_1 = A_2$ and $A_3$, bulk and shear anisotropy factors (%), acoustic Grüneisen parameter, and melting temperature (in K) of $V_2Ni_2Z'Z''$ compounds.

| Compounds | $B$ | $G$ | $E$ | $\nu$ | $B/G$ | $H_V$ | $K_{IC}$ | $A_1 = A_2$ | $A_3$ | $A_B$ | $A_G$ | $\gamma^{ac}$ | $T_m$ |
|---|---|---|---|---|---|---|---|---|---|---|---|---|---|
| $V_2Ni_2AlSb$ | 133.86 | 56.09 | 147.65 | 0.316 | 2.38 | 5.28 | 2.33 | 1.066 | 0.960 | 0.008 | 0.068 | 1.87 | 1287 |
| $V_2Ni_2AlSn$ | 136.37 | 59.79 | 156.46 | 0.309 | 2.28 | 5.93 | 2.42 | 0.965 | 0.954 | 0.002 | 0.019 | 1.82 | 1335 |
| $V_2Ni_2GaSb$ | 135.78 | 53.08 | 140.89 | 0.327 | 2.56 | 4.54 | 2.28 | 1.166 | 1.056 | 0.001 | 0.229 | 1.95 | 1261 |
| $V_2Ni_2GaSn$ | 138.50 | 57.88 | 152.40 | 0.317 | 2.39 | 5.38 | 2.40 | 1.056 | 1.065 | 0.001 | 0.040 | 1.89 | 1313 |

importance of V *d*-states in shaping the electronic properties of the $V_2Ni_2AlSb$ and $V_2Ni_2AlSn$ alloys. A similar electronic state configuration is also observed in the related alloys $V_2Ni_2GaSb$ and $V_2Ni_2GaSn$, suggesting a consistent influence of V *d*-states across these systems in establishing half-metallic behavior.

To investigate the various interactions and bonding characteristics in the selected DHH alloys, we calculated and analyzed the electron localization function (ELF), particularly within the (110) crystallographic plane. As illustrated in Fig. 6, the alloys under investigation can be structurally divided into three main layers based on the distribution of electron density. The first layer consists of V atoms. The second layer contains Ni atoms that form V–Ni bonds. Finally, the third layer comprises elements Z′ (Al, Ga) and Z″ (Sb, Sn). Analysis of the electron localization function reveals that V–Ni bonds have low electronic localization, indicating weak covalent interactions (0.4). In contrast, Ni–Al bonds show the highest degree of electronic localization, corresponding to strong covalent bonding (≈0.8). Despite the spatial separation of Sb and Al atoms in the Z′ and Z″ layer, a moderate level of electronic localization is observed (≈0.5), indicating an intermediate covalent interaction between these elements. This bonding nature is consistent across all the studied alloys. In alloys containing Sb (a and c), covalent bonding is dominant, accompanied by a high degree of electron localization. In contrast, Sn-based alloys (b and d) have a reduced proportion of covalent interactions and a lower degree of electron localization. The replacement of Al with Ga induces minimal changes in the bonding characteristics, while replacing Sb with Sn significantly weakens the covalent interactions. These results suggest that the bonding in double Heusler alloys is primarily determined by the electronic structures of the Z′ and Z″ elements.

### D. Elastic properties

In the tetragonal crystal structure of the double half-Heusler alloy, six independent elastic constants were identified: $C_{11}$, $C_{12}$, $C_{13}$, $C_{33}$, $C_{44}$, and $C_{66}$. These constants were selected to fully characterize the elastic properties of the material. Table IV provides the calculated values of the elastic constants $C_{ij}$ for each of the four studied compounds.

In Table V using the calculated elastic constants, the elastic moduli such as the bulk modulus, shear modulus, Young modulus, and Poisson ratio can be evaluated. The $V_2Ni_2AlSn$ and $V_2Ni_2GaSn$ alloys exhibited high values of Young's modulus, indicating that these materials are characterized by high stiffness and exhibit limited elastic deformation. The Poisson ratio, which allows for an estimation of the material's volumetric deformation characteristics, specifically the extent of transverse dimensional change under tensile or compressive loading, exhibits a high value for the $V_2Ni_2GaSb$ alloy. For the $V_2Ni_2GaSb$ alloy, the Vickers hardness $H_V$ is the lowest at 4.54 GPa, while the highest value, 5.93 GPa, is observed for the $V_2Ni_2AlSn$ alloy, with intermediate values found

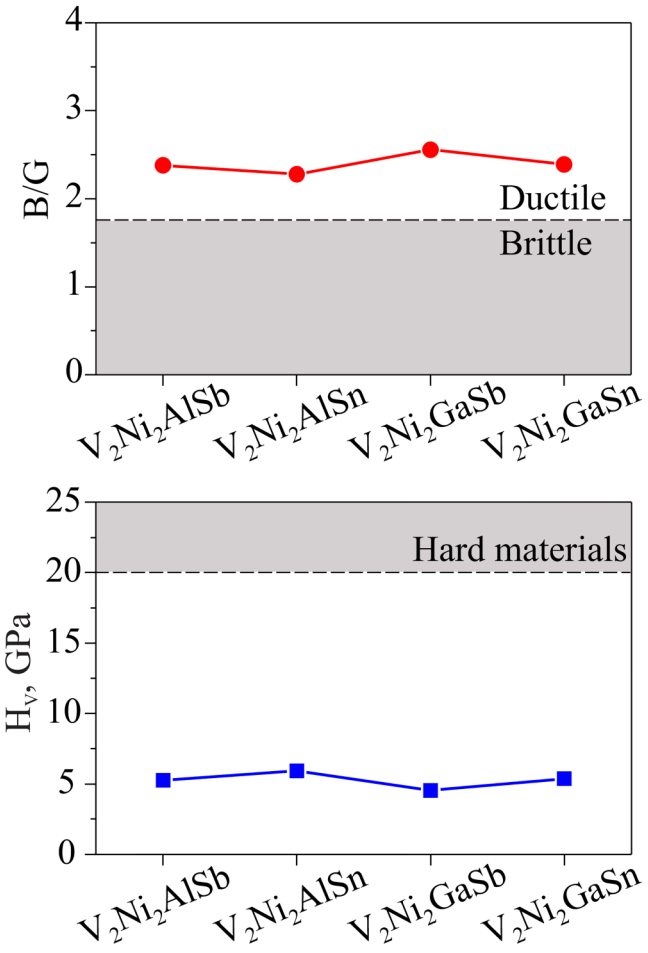


**FIG. 7.** Comparative analysis of values of hardness ($H_V$), $B/G$ for $V_2Ni_2Z'Z''$ compounds.

for the remaining alloys. Notably, all hardness values fall below the minimum threshold typically expected for hard materials ($H_V > 20$ GPa). For clarity, Fig. 7 presents the calculated hardness values in comparison with the minimum standard for hard materials. A $B/G$ ratio greater than 1.75 typically indicates ductility, whereas a ratio below 1.75 suggests the brittle nature of a material. In the present study, the $B/G$ ratios are relatively high (≈2.5), which signifies that the materials exhibit ductile behavior. Based on the calculated bulk and shear moduli, the elastic anisotropy was determined for both the bulk modulus $A_B$ and the shear modulus $A_G$. For a perfectly isotropic material, the anisotropy value is 0%, while a value of 100% represents maximum anisotropy. The analysis of the results reveals that the selected alloys exhibit values close to isotropic. The calculation of shear anisotropy factors is crucial for assessing the material's durability, as they are primarily associated with the formation and propagation of microcracks in the crystal structure. So $A_1 = A_2$ for the {100} and {010} planes between the ⟨011⟩, ⟨010⟩, and ⟨101⟩, ⟨001⟩ directions, and $A_3$ for the {001} shear planes between ⟨110⟩ and ⟨010⟩ directions were calculated.[44,45] We have also determined the Grüneisen parameter $\gamma^{ac}$, which is a crucial quantity for characterizing the thermodynamic properties of solids. The Grüneisen parameter serves as an effective measure of the anharmonicity of atomic and molecular interactions within a material and influences various fundamental physical processes. This is known as the "acoustical" Grüneisen parameter and is defined by the measured sound velocities $v_l$ and $v_t$.[21] The Grüneisen parameter for the investigated alloys is approximately (1.9), with the highest value observed for $V_2Ni_2GaSb$ (1.95).

## IV. CONCLUSION

This comprehensive study of $V_2Ni_2Z'Z''$ (where Z′ = Al, Ga and Z″ = Sb, Sn) double half-Heusler alloys has demonstrated that these materials possess a favorable combination of electronic, magnetic, elastic, and dynamic properties, positioning them as promising candidates for advanced technological applications, particularly in the field of spintronics. By employing the DFT calculations, the mechanical, dynamic, and thermodynamic stability of each alloy were demonstrated. It was shown that all compounds adhere to the Slater–Pauling rule. The magnetic analysis revealed that the $V_2Ni_2AlSb$ and $V_2Ni_2GaSb$ alloys exhibit ferromagnetic properties, while $V_2Ni_2AlSn$ and $V_2Ni_2GaSn$ are ferrimagnetic, allowing for potential magnetic tunability in device applications. Electronic property analysis indicated that each alloy exhibits half-metallicity, with an energy gap in the spin-up channel ranging from 0.103 to 0.653 eV, supporting their suitability for spintronic applications. Mechanical analysis revealed high stiffness in $V_2Ni_2AlSn$ and $V_2Ni_2GaSn$, as evidenced by their elevated Young's modulus values, while the relatively high Poisson's ratio of $V_2Ni_2GaSb$ suggests substantial volumetric deformation potential under load. Although the Vickers hardness values (4.54–5.93 GPa) fall below the threshold for traditional hard materials, they remain appropriate for applications requiring moderate hardness. Furthermore, all alloys exhibit ductile behavior, as indicated by the $B/G$ ratio values (approximately 2.5), and near-isotropic properties based on elastic anisotropy calculations. The results of this study underscore the potential of $V_2Ni_2Z'Z''$ alloys for integration into spintronic devices and other advanced technologies, combining the benefits of half-metallicity, magnetic tunability, and mechanical resilience. These findings contribute valuable insights into developing robust, high-performance materials for next-generation technological applications.

## ACKNOWLEDGMENTS

This study was funded by the Ministry of Science and Higher Education of the Republic of Kazakhstan under the "Zhas Galym" project under No. 2024-2026 AP22683528 "Computer design of thermoelectric and spintronic materials based on Heusler alloys." V.V.K. acknowledges the Priority-2030 program of NUST MISIS under Grant No. K2-2022-022. The calculations were performed using resources provided by the Novosibirsk State University Supercomputer Center. N.E.S. was supported by the state assignment of IGM SB RAS (No. 122041400176-0). The work by TMI was carried out within the state assignment of the Vernadsky Institute of Geochemistry and Analytical Chemistry of the Russian Academy of Sciences (GEOKHI RAS).

## AUTHOR DECLARATIONS

### Conflict of Interest

The authors have no conflicts to disclose.

### Author Contributions

**Nurpeiis A. Merali:** Data curation (equal); Funding acquisition (equal); Writing – original draft (equal). **Nurgul S. Soltanbek:** Data curation (equal); Writing – original draft (equal). **Nursultan E. Sagatov:** Methodology (lead); Supervision (equal); Writing – review & editing (equal). **Aisulu U. Abuova:** Project administration (equal): Visualization (equal). **Vladimir V. Khovaylo:** Project administration (equal); Resources (lead); Visualization (equal). **Fatima U. Abuova:** Project administration (equal); Resources (lead); Visualization (equal). **Talgat M. Inerbaev:** Conceptualization (equal); Supervision (equal); Writing – review & editing (equal).



## DATA AVAILABILITY

The data that support the findings of this study are available within the article.

## REFERENCES

[1]W. G. Zeier, J. Schmitt, G. Hautier, U. Aydemir, Z. M. Gibbs, C. Felser, and G. J. Snyder, "Engineering half-Heusler thermoelectric materials using Zintl chemistry," Nat. Rev. Mater. **1**, 1–10 (2016).
[2]S. Anand, M. Wood, Y. Xia, C. Wolverton, and G. J. Snyder, "Double half-Heuslers," Joule **3**, 1226–1238 (2019).
[3]P. J. Webster, "Heusler alloys," Contemp. Phys. **10**, 559–577 (1969).
[4]K. Elphick, W. Frost, M. Samiepour, T. Kubota, K. Takanashi, H. Sukegawa, S. Mitani, and A. Hirohata, "Heusler alloys for spintronic devices: Review on recent development and future perspectives," Sci. Technol. Adv. Mater. **22**, 235–271 (2021).
[5]S. Tavares, K. Yang, and M. A. Meyers, "Heusler alloys: Past, properties, new alloys, and prospects," Prog. Mater. Sci. **132**, 101017 (2023).
[6]F. Abuova, T. Inerbaev, A. Abuova, N. Merali, N. Soltanbek, G. Kaptagay, M. Seredina, and V. Khovaylo, "Structural, electronic and magnetic properties of

$Mn_2Co_{1-x}V_xZ$ (Z = Ga, Al) Heusler alloys: An insight from DFT study," Magnetochemistry **7**, 159 (2021).
[7]A. Abuova, N. Merali, F. Abuova, V. Khovaylo, N. Sagatov, and T. Inerbaev, "Electronic properties and chemical bonding in $V_2FeSi$ and $Fe_2VSi$ Heusler alloys," Crystals **12**, 1546 (2022).
[8]Y. Rached, M. Caid, M. Merabet, S. Benalia, H. Rached, L. Djoudi, M. Mokhtari, and D. Rached, "A comprehensive computational investigations on the physical properties of TiXSb (X: Ru, Pt) half-Heusler alloys and $Ti_2RuPtSb_2$ double half-Heusler," Int. J. Quantum Chem. **122**, e26875 (2022).
[9]R. Hasan, T. Park, S.-I. Kim, H.-S. Kim, S. Jo, and K. H. Lee, "Enhanced thermoelectric properties of $Ti_2FeNiSb_2$ double half-Heusler compound by Sn doping," Adv. Energy Sust. Res. **3**, 2100206 (2022).
[10]M. A. Hassan, A. El-Khouly, E. Elsehly, E. N. Almutib, S. K. Elshamndy, I. Serhiienko, E. Argunov, A. Sedegov, D. Karpenkov, D. Pashkova *et al.*, "Transport and thermoelectric properties of melt spinning synthesized $M_2FeNiSb_2$ (M = Ti, Hf) double half Heusler alloys," Mater. Res. Bull. **164**, 112246 (2023).
[11]Z. Charifi, H. Baaziz, Ş. Uğur, and G. Uğur, "Prediction of the electronic structure, optical and vibrational properties of $ScXCo_2Sb_2$ (X = V, Nb and Ta) double half-Heusler alloys: A theoretical study," Indian J. Phys. **97**, 413–428 (2023).
[12]M. Boudjelal, K. Bouhadjer, M. Matougui, S. Bentata, V. Srivastata, S. Bin-Omran, and R. Khenata, "Ab initio prediction of the structural, optoelectronic and thermoelectric properties of double half-Heusler (DHH) $ScXRh_2Bi_2$ (X= Nb, Ta) alloys DFT study results," Indian J. Phys. **98**, 3141–3154 (2024).
[13]M. Mekhtiche, M. Matougui, M. Houari, B. Bouadjemi, T. Lantri, M. Boudjelal, and S. Bentata, "Predictive study of the new double half-Heusler compounds $Hf_2FeNiSb_2$, $Nb_2Co_2GaSb$ and $ScNbCo_2Sb_2$, promising candidates for thermoelectric applications," Indian J. Phys. **98**, 3121–3129 (2024).
[14]M. Diaf, H. Righi, H. Rached, D. Rached, and R. Beddiaf, "Ab initio study of the properties of $Ti_2PdFe$ (Ru) $Sb_2$ double half-Heusler semiconducting alloys," J. Electron. Mater. **52**, 6514–6529 (2023).
[15]K. Bouhadjer, M. Boudjelal, M. Matougui, S. Bentata, T. Lantri, M. Batouche, T. Seddik, R. Khenata, B. Bouadjemi, S. B. Omran *et al.*, "Structural, optoelectronic, thermodynamic and thermoelectric properties of double half-Heusler (DHH) $Ti_2FeNiSb_2$ and $Ti_2Ni_2InSb$ compounds: A TB-mBJ study," Chin. J. Phys. **85**, 508–523 (2023).
[16]H. Ding, X. Li, Y. Feng, and B. Wu, "Electronic structure, magnetism and disorder effect in double half-Heusler alloy $Mn_2FeCoSi_2$," J. Magn. Magn. Mater. **555**, 169367 (2022).
[17]O. Douinat, A. Boucherdoud, A. Seghier, M. Houari, S. Mesbah, T. Lantri, and B. Bestani, "Theoretical investigation of the physical, mechanical, and thermal properties of $Zr_2XBiNi_2$ (X: Al, Ga) double half-Heusler alloys," J. Mater. Res. **38**, 4509–4521 (2023).
[18]Z. Cui, H. Ding, and Y. Feng, "Investigation of the half-metallicity, magnetism and spin transport properties of double half-Heusler alloys $Mn_2$ $CoCrZ_2$ (Z = P, As)," Phys. Chem. Chem. Phys. **23**, 17984–17991 (2021).
[19]H. Mekki, H. Baaziz, Z. Charifi, T. Ghellab, A. Genç, Ş. Uğur, and G. Uğur, "Properties of the double half-Heusler alloy $ScNbNi_2Sn_2$ with respect to structural, electronic, optical, and thermoelectric aspects," Solid State Commun. **363**, 115103 (2023).
[20]S. S. Essaoud, A. Bouhemadou, D. Allali, M. E. Ketfi, M. Radjai, and S. Bin-Omran, "An ab initio investigation of the structural stability, thermodynamic, optoelectronic, and thermoelectric properties of $LuXNi_2Sn_2$ (X = V, Nb, Ta) double half Heusler materials," J. Inorg. Organomet. Polym. Mater. **34**, 885–902 (2024).
[21]M. Diaf, H. Righi, R. Beddiaf, Y. Djaballah, and H. Rached, "Ab initio investigation of the structural, mechanical, electronic, thermodynamic, and optical properties of $V_2FeNiGe_2$ and $Hf_2FeNiSb_2$ double half-Heusler compounds," Can. J. Phys. **103**, 288–301 (2024).
[22]X. Liu, S. Wang, Z. Dong, Y. Chang, J. Zhang, X. Zhang, and J. Luo, "Discovery of (Sc, V) CoSb double half-Heusler alloys with low lattice thermal conductivity," J. Alloys Compd. **1010**, 178078 (2025).
[23]K. Imasato, P. Sauerschnig, M. Miyata, T. Ishida, A. Yamamoto, and M. Ohta, "Effects of the Fe/Ni ratio in double half-Heusler composition $HfFe_{1-x}Ni_xSb$," J. Mater. Chem. C **13**, 2154–2164 (2025).
[24]G. Kresse and J. Furthmüller, "Efficient iterative schemes for ab initio total-energy calculations using a plane-wave basis set," Phys. Rev. B **54**, 11169–11186 (1996).
[25]G. Kresse and J. Furthmüller, "Efficiency of ab-initio total energy calculations for metals and semiconductors using a plane-wave basis set," Comput. Mater. Sci. **6**, 15–50 (1996).
[26]G. Yergaliuly, A. Tangirbergen, A. Mentbayeva, N. Amangeldi, M. Kaikanov, S. Acar, Z. Bakenov, and B. Soltabayev, "Advanced surface engineering of TZO nanostructures via irradiation technique for enhanced nitric oxide (NO) gas sensitivity," Appl. Surf. Sci. Adv. **27**, 100736 (2025).
[27]N. S. Soltanbek, N. A. Merali, N. E. Sagatov, F. U. Abuova, E. Elsts, A. U. Abuova, V. V. Khovaylo, T. M. Inerbaev, M. Konuhova, and A. I. Popov, "Ab initio investigation of the stability, electronic, mechanical, and transport properties of new double half Heusler alloys $Ti_2Pt_2ZSb$ (Z = Al, Ga, In)," Metals **15**, 329 (2025).
[28]A. Tangirbergen, N. Amangeldi, S. T. Revankar, and G. Yergaliuly, "A review of irradiation-induced hardening in FeCrAl alloy systems for accident-tolerant fuel cladding," Nucl. Eng. Des. **429**, 113659 (2024).
[29]Z. M. Salikhodzha, G. B. Bairbayeva, R. N. Kassymkhanova, M. Konuhova, K. B. Zhangylyssov, E. Popova, and A. I. Popov, "Density functional theory study of pressure-dependent structural and electronic properties of cubic zirconium dioxide," Ceramics **8**, 41 (2025).
[30]Z. Salikhodzha, T. Nurakhmetov, A. Popov, A. Z. Kainarbay, A. Akhmedov, and F. Abuova, "First principles calculations of the electronic structure and processes of formation of defects in the $Na_2SO_4$ crystal," Opt. Mater.: X (published online 2025).
[31]J. P. Perdew, K. Burke, and M. Ernzerhof, "Generalized gradient approximation made simple," Phys. Rev. Lett. **77**, 3865 (1996).
[32]J. Sun, R. C. Remsing, Y. Zhang, Z. Sun, A. Ruzsinszky, H. Peng, Z. Yang, A. Paul, U. Waghmare, X. Wu *et al.*, "Accurate first-principles structures and energies of diversely bonded systems from an efficient density functional," Nat. Chem. **8**, 831–836 (2016).
[33]A. Togo and I. Tanaka, "First principles phonon calculations in materials science," Scr. Mater. **108**, 1–5 (2015).
[34]W. Voigt, *Lehrbuch der Kristallphysik (Textbook of Crystal physics)* (BG Teubner, Leipzig, 1928).
[35]A. Reuss, "Calculation of the flow limits of mixed crystals on the basis of the plasticity of monocrystals," Z. Angew. Math. Mech. **9**, 49–58 (1929).
[36]R. Hill, "The elastic behaviour of a crystalline aggregate," Proc. Phys. Soc. Sect. A **65**, 349 (1952).
[37]R. Hill, "Elastic properties of reinforced solids: Some theoretical principles," J. Mech. Phys. Solids **11**, 357–372 (1963).
[38]H. Chen, L. Yang, and J. Long, "First-principles investigation of the elastic, Vickers hardness and thermodynamic properties of Al–Cu intermetallic compounds," Superlattices Microstruct. **79**, 156–165 (2015).
[39]S. I. Ranganathan and M. Ostoja-Starzewski, "Universal elastic anisotropy index," Phys. Rev. Lett. **101**, 055504 (2008).
[40]M. Fine, L. Brown, and H. Marcus, "Elastic constants versus melting temperature in metals," Scr. Metall. **18**, 951–956 (1984).
[41]A. Belkacem, H. Rached, M. Caid, Y. Rached, D. Rached, N. T. Mahmoud, and N. Benkhettou, "The stability analysis and efficiency of the new MAX-phase compounds $M_3GaC_2$ (M: Ti or Zr): A first-principles assessment," Results Phys. **38**, 105621 (2022).
[42]X.-Q. Chen, H. Niu, D. Li, and Y. Li, "Modeling hardness of polycrystalline materials and bulk metallic glasses," Intermetallics **19**, 1275–1281 (2011).
[43]Y. Tian, B. Xu, and Z. Zhao, "Microscopic theory of hardness and design of novel superhard crystals," Int. J. Refract. Met. Hard Mater. **33**, 93–106 (2012).
[44]H. Rached, D. Rached, S. Benalia, A. Reshak, M. Rabah, R. Khenata, and S. B. Omran, "First-principles study of structural stabilities, elastic and electronic properties of transition metal monocarbides (TMCs) and mononitrides (TMNs)," Mater. Chem. Phys. **143**, 93–108 (2013).
[45]Z. E. Biskri, H. Rached, M. Bouchear, and D. Rached, "Computational study of structural, elastic and electronic properties of lithium disilicate ($Li_2Si_2O_5$) glass-ceramic," J. Mech. Behav. Biomed. Mater. **32**, 345–350 (2014).